Hindawi
Advances in Civil Engineering
Volume 2018, Article ID 1634702, 10 pages
https://doi.org/10.1155/2018/1634702

Research Article

A New Rate-Dependent Constitutive Model of Superelastic Shape Memory Alloys and Its Simple Application in a Special Truss Moment Frame Simulation

Maria I. Ntina and Dimitrios S. Sophianopoulos

Department of Civil Engineering, University of Thessaly, Volos 38334, Greece

Correspondence should be addressed to Dimitrios S. Sophianopoulos; dimsof@civ.uth.gr

Received 17 June 2018; Revised 9 August 2018; Accepted 13 August 2018; Published 17 September 2018

Academic Editor: Rosario Montuori

In this work, a new constitutive model of the behavior of shape-memory alloys is presented, based on earlier models, showing a very good agreement with the existing experimental results. A simple approximate application concerning the use of these alloys modelled as dissipation devices in a special truss-moment frame is demonstrated. The results obtained are considered sufficiently encouraging as a motivation for the ongoing work.

1. Introduction

Shape-memory alloys (SMAs) are unique materials having the ability to recover their original shape after mechanical distortion via the application of heat, which indicates the shape-memory effect, or by unloading, which indicates the superelastic effect, through the phase change (austenitic-martensitic). This ability has made SMAs quite popular for a wide variety of applications, such as aerospace, automotive, dental, biomedical, and, of course, structural. An interesting review of the use of SMAs in civil engineering is the one by Song et al. [1]; this use concerns passive structural control, energy dissipation devices, shape restoration, active structural frequency tuning, self-rehabilitation, etc.

In the literature, a limited number of SMA constitutive (behavioral) models have been reported [2] but to some extent, as it will be explained in the later section, all possess flaws and drawbacks in fully describing both the aforementioned effects. In order to overcome these drawbacks, in the present work, a new rate-dependent constitutive model for superelastic SMAs is presented, which is found to have very good agreement with the experimental results.

Finally, a preliminary investigation on the potential use of this model as an energy dissipation device in the special segments of steel special truss moment frames [3, 4] is offered. This is performed by considering a simple 2-DOF simulation of such frames and studying its dynamic response under various types of time-dependent lateral loads.

2. SMA Features and Existing Behavioral (Constitutive) Models

In this section, an overview of the features and characteristics of SMAs is presented, as well as a short description of the most relevant constitutive models. This is considered needed to allow the reader to comprehensively follow the subject of the present work.

2.1. SMA Features and Characteristics. Shape-memory alloys (SMAs) are unique materials having the ability to recover their original shape after mechanical distortion via the application of heat, which indicates the shape-memory effect, or by unloading, which indicates the superelastic effect, through the phase change (austenitic-martensitic).

SMAs have the ability to form two crystal structures through the rearrangement of atoms within the crystal lattice, the austenitic and the martensitic. Their features are

the consequences of shape changes due to martensitic phase transformations. This kind of transformations is reversible diffusionless shear transformations which occur by some form of cooperative movement of a relatively large number of atoms, each being displaced by a small distance relative to its neighbours and that results in a change in the crystal structure. The diffusionless character makes the martensitic transformation almost instantaneous.

The austenitic crystal structure, which SMAs form, is characterized by a cubic high-symmetry structure stable at higher temperatures, whereas the martensitic one by a monoclinic low-symmetry structure is stable at lower temperatures. The austenitic phase is called the "parent" phase, and it presents only one crystal-orientation direction, which is called a variant, whereas the martensitic phase presents twenty-four variants, and their structure depends on the type of the transformation the material has undergone. This is because, when the austenite shears to form the martensite, there are different directions to do this.

In a stress-free state, an SMA is characterized by four transformation temperatures: M_s, M_f, A_s, and A_f. The first two, with M_s smaller than M_f, indicate the temperatures at which the transformation of austenite to martensite starts and finishes during cooling. The latter, with A_s smaller than A_f, is the temperatures at which the transformation of martensite into austenite starts and finishes during heating.

The loading and unloading of an SMA in the austenitic state results in a hysteresis loop with zero or insignificant residual strain. This is due to the fact that the austenitic phase is loaded elastically up to a "yield" stress where a stress-induced transformation from austenite to martensite takes place. The martensite that is formed due to the application of stress is called detwinned martensite or stress-induced martensite, and its formation process consists of the spatial re-orientation of the original martensite variants. The product phase is then called a single-variant martensite and is characterized by a detwinned structure [2]. During transformation, the proportion of the specimen that has been transformed to martensite progressively rises. This occurs without much increase in the stress, and the stress-strain curve follows a stress plateau until the martensite is fully detwinned.

After the complete transformation to martensite, further straining causes its elastic loading at a modulus lower than that of elastic austenite but much higher than that of the phase transition portion of the loading curve. Upon unloading, since martensite is stable due to the presence of the applied stress, the reverse transformation takes place but at a lower stress plateau. After full unloading, the material ideally returns to its undeformed geometry [5]. Overall, the loop presents high stiffness for small strain levels, reduced stiffness for intermediate levels of strain due to the formation of martensite, and high stiffness at large levels of strain due to the elastic loading of martensite. Also, it usually exhibits higher critical transformation stress and smaller reverse transformation stress due to the strong orientation dependence of the martensitic transformation.

There are limits to stress ranges among which superelastic deformation can occur. Excessive deformation beyond that, which can be accommodated by transformation to martensite, will lead to plastic deformation by slip, which is an irreversible process.

A typical schematic picture of a superelastic loading path is presented in Figure 1, whereas a corresponding stress-strain curve is depicted in Figure 2.

2.2. Models of SMA Behavior. Buehler et al. [7], while investigating materials useful for heat shielding, discovered the special nature of SMAs in the 1960s at the U.S. Naval Ordnance Laboratory in the early phases of research on the 55-nitinol alloys. It was noticed that apart from their good mechanical properties, they possessed a shape recovery capability. Some other aspects, such as the damping change in relation to temperature, the composition of the alloy, and the temperature and the mode of plastic deformation, began at that time to attract the interest of researchers.

Since then, the first serious attempt to develop a rational force-displacement relationship for a metallic damper was made by Özdemir [8], who in his PhD thesis proposed a rate-independent model, considering it as superior than earlier rate-dependent ones in reproducing the behavior of energy absorbers. Later, Graesser and Cozzarelli [5] modified Özdemir's model, in order to capture the behavior of SMAs due to both shape-memory and superelastic effects. A few years later, other models were also presented in the literature, such as the ones by Wilde et al. [9] and Auricchio et al. [10]. We will focus on a short description of the model given in [5] since the one developed herein is based on it.

In this particular model of interest, the equation of the stress was identical to the one by Özdemir given as follows:

$$\dot{\sigma} = E\left[\dot{\varepsilon} - \dot{\varepsilon}\left(\frac{\sigma-\beta}{\gamma}\right)^{n}\right], \tag{1}$$

where E is the Young's modulus of elasticity, $\dot{\varepsilon}$ is the strain rate, β is the back stress, Y is the "yield" stress, and η is a constant controlling the sharpness of transition from elastic to plastic states. The expression of the back stress is as follows:

$$\beta = E\alpha\left\{\varepsilon^{\text{in}} + f_t|\varepsilon|^{c}\ \text{erf}\,(a\varepsilon)[u(-\varepsilon\dot{\varepsilon})]\right\}, \tag{2}$$

in which a is a constant controlling the slope of the stress-strain curve, being equal to

$$\alpha = \frac{E_y}{E - E_y}, \tag{3}$$

with E_y as the after-yielding modulus while the inelastic strain ε^{in} in Equation (2) is

$$\varepsilon^{\text{in}} = \varepsilon - \frac{\sigma}{E}. \tag{4}$$

Parameters f_t, c, and a are material constants. The constant f_t is included in order to allow for the patterns of hysteretic behavior observed in SMAs, namely, the shape-memory and the superelastic effects. Notations erf () and u() are used to represent the error function and the unit step function, respectively. These two functions are defined as

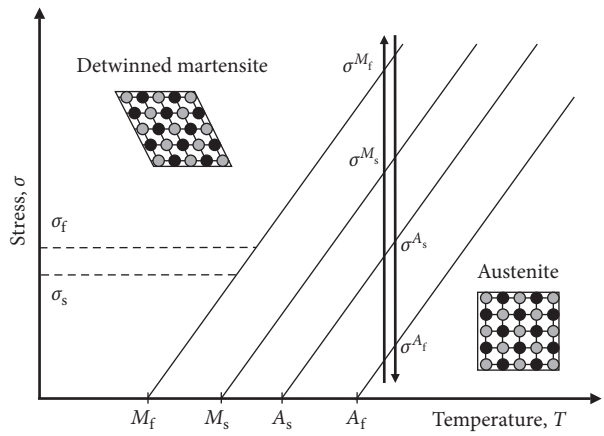

Figure 1: A superelastic loading path (from Lagoudas [6]).

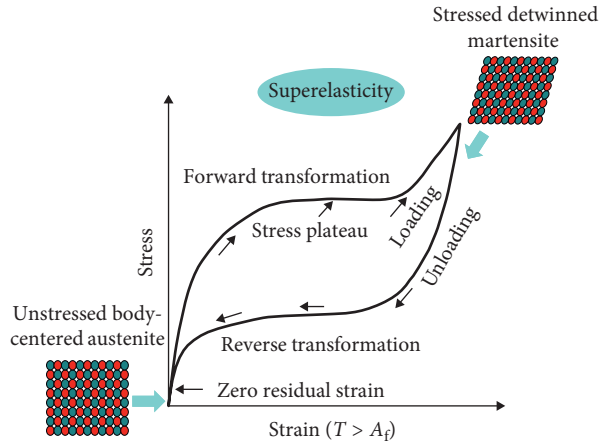

Figure 2: Schematic stress-strain curve of superelastic effect of SMAs.

$$\operatorname{erf}(x) = \frac{2}{\sqrt{\pi}} \int_0^x e^{-t^2} dt,$$
$$u(x) = \left\{ \begin{array}{l} 1, \quad x \geq 0 \\ \\ 0, \quad x < 0 \end{array} \right\}. \tag{5}$$

The unit-step function will activate the added term of the expression of the back stress only during unloading. The branch of the hysteresis loop during loading is unaffected by it. The motivation for selecting this particular form of the back stress arises from the requirement of zero residual strain, which is necessary when describing superelastic material behavior. For a superelastic type of response, parameters f_t, c, and a are chosen such that the back stress will exceed the stress at the onset of unloading, and this will cause the inelastic strain to decrease.

If the parameter f_t is chosen to be zero, the shape generated by the model resembles the curves generated by Özdemir's model, which corresponds to the shape-memory effect response. A typical representation of the foregoing model's cyclic response, for both effects, is shown in Figure 3.

3. The New SMA Constitutive Model-Proposed Theory and Comparative Results

A feasible SMA constitutive model must be able to represent (a) the elastic loading of martensite that follows the complete transformation of austenite to martensite in a superelastic type of response and (b) the rate-dependent nature.

All the models referenced above, more or less, have some serious drawbacks. More specifically, the ones presented by Özdemir [8] and Graesser and Cozzarelli [5] cannot take under consideration the rate-dependent nature of SMA and the elastic loading of martensite. Furthermore, Wilde et al. [9] indeed attempted to simulate the elastic loading of martensite, developing nonetheless, another rate-independent model. Finally, Auricchio et al. [10] managed to capture all the above requirements, but their model is quite complicated and difficult to implement.

In the sequel, a new constitutive model is presented herein, in order to capture the aforementioned characteristics of SMAs; it is based on Graesser-Cozzarelli model, as previously stated.

The stress exerted on the SMA is the stress σ of Equation (1) of Graesser–Cozzarelli model while the back stress β involves the addition of two more terms in Equation (2), namely, σ_1 and σ_2, as explained in what follows. Thus, we can write that

$$\beta_{\text{tot}} = \beta + \sigma_1 + \sigma_2. \tag{6}$$

In order to determine the form of σ_1 and σ_2 stresses, data from experiments conducted by DesRoches et al. [11] on 7.1 mm diameter bars under cyclic loading, which causes stable strain rate at frequencies of 0.025 Hz, 0.5 Hz, and 1 Hz, were used. Comparing the stress-strain curves obtained from the experiment for these three frequencies, the rate-dependent nature of the SMAs is revealed.

In Figure 4, one may perceive the digitized experimental data given in [11], plotted as full cyclic tests, in order to aid the representation of the model; the continuous part of the curves were reported while the dotted parts were not since half cycle tests were conducted.

As depicted in Figure 4, there is a significant change of the SMA behavior between the response at the frequency of 0.025 Hz and the one at 0.5 Hz. Passing to frequencies of seismic interest, the loop becomes more narrow, and the loading and the unloading stresses increase. The response between the frequencies of 0.5 and 1 Hz seems to have insignificant differences.

Figure 5 shows a comparison between Graesser–Cozzarelli model prediction and the experiment for a static loading frequency of 0.025 Hz using the following model parameter values: $E = 35$ GPa, $Y = 300$ MPa, $\eta = 7$, $\alpha = 0.0488$, $f_t = 0.268$, $c = 0.002$, and $a = 165$. The behavior of the SMA bar was generally well captured by the model, except the elastic loading of martensite, since the behavior at this frequency is not affected by the strain rate.

Moreover, comparing the Graesser–Cozzarelli model prediction to the experimental stress-strain curve at frequencies of 0.5 and 1 Hz, a significant difference is observed

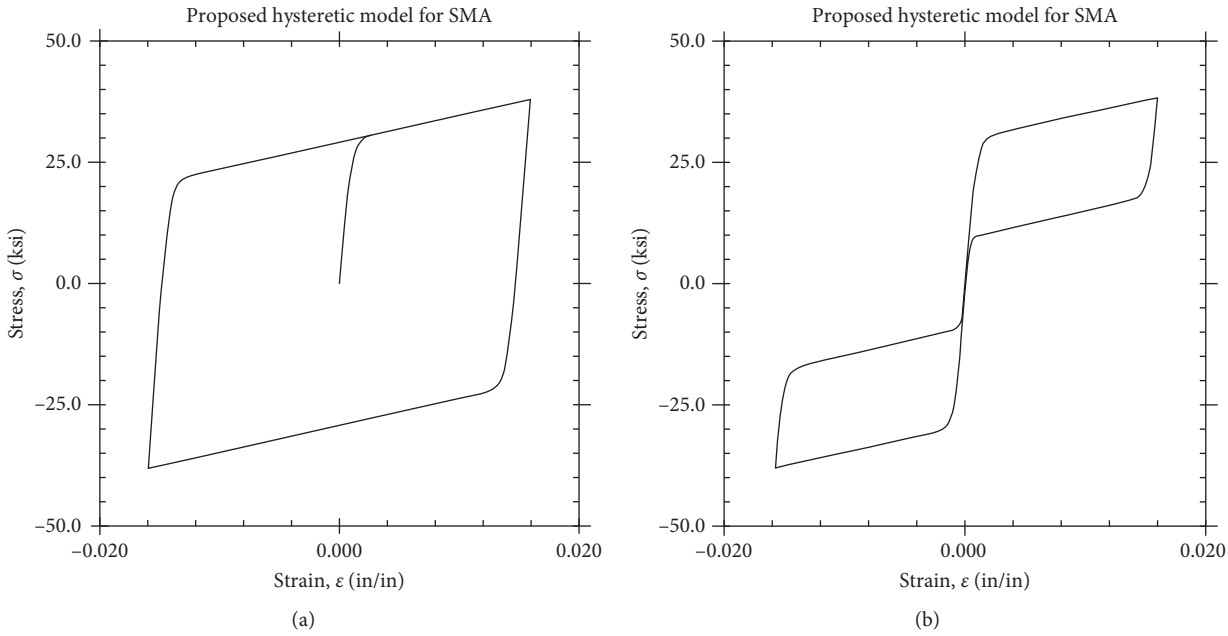

Figure 3: Typical cyclic response of Graesser– Cozzarelli model for (a) $f_t = 0$ (shape-memory effect) and (b) $f_t \neq 0$ (superelastic effect).

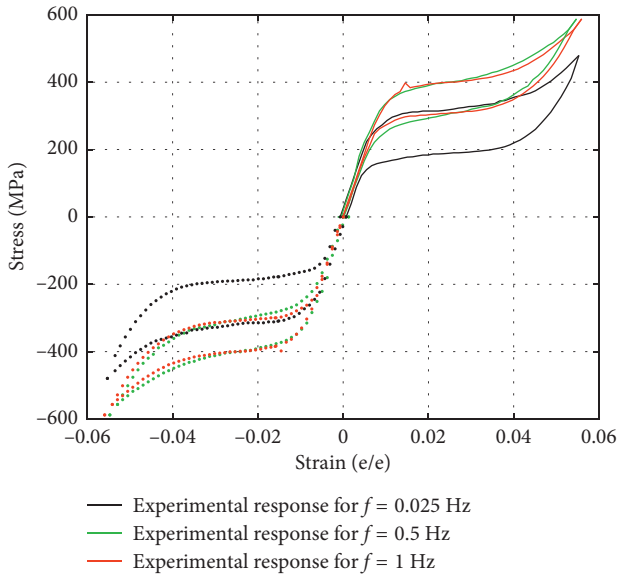

Figure 4: Comparison of the experimental responses at frequencies of 0.025, 0.5, and 1 Hz.

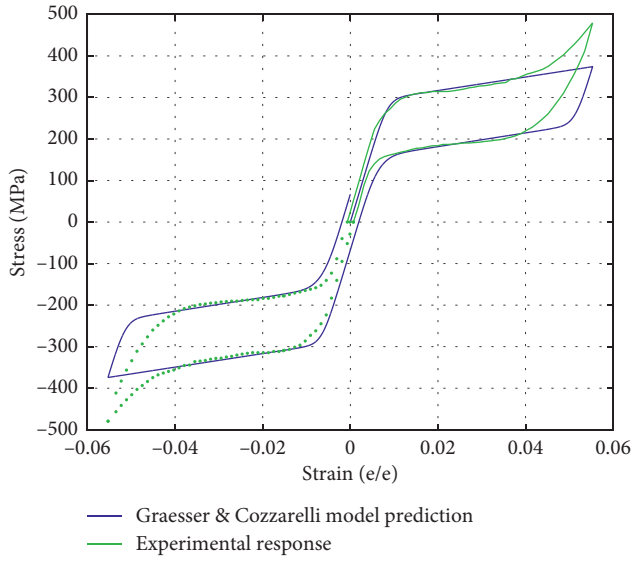

Figure 5: Comparison of Graesser–Cozzarelli model prediction to experimental response at $f = 0.025$ Hz.

due to the rate-independent character of the model. The behavior predicted is the same for any frequency as shown in Figure 6.

According to the above comparisons, we may then proceed to the definitions of the additional stresses of Equation (6). As far as stress σ_1 is concerned and in order to capture the martensite phase of the material, it is introduced in the form of

$$\sigma_1 = \frac{\Delta\sigma_1}{\Delta\varepsilon} \operatorname{sign}(\varepsilon)(|\varepsilon| - 0.04), \tag{7}$$

where $\Delta\sigma_1$ is the stress difference between the stress plateau during forward transformation (or the stress at the end of the martensitic phase) and the stress at the maximum strain (beyond martensitic phase) from the experimental response at a frequency of 0.025 Hz while $\Delta\varepsilon$ is the corresponding strain difference. The elastic loading of the martensitic phase is supposed to start beyond 4% strain. In order to capture the effect of the strain rate, we proceed with the introduction of stress σ_2 of Equation (6), which is written as

$$\sigma_2 = \Delta\sigma_2 \operatorname{sign}(\varepsilon)[|\varepsilon|]^{\left|\dot{\varepsilon}_0/\dot{\varepsilon}\right|}, \tag{8}$$

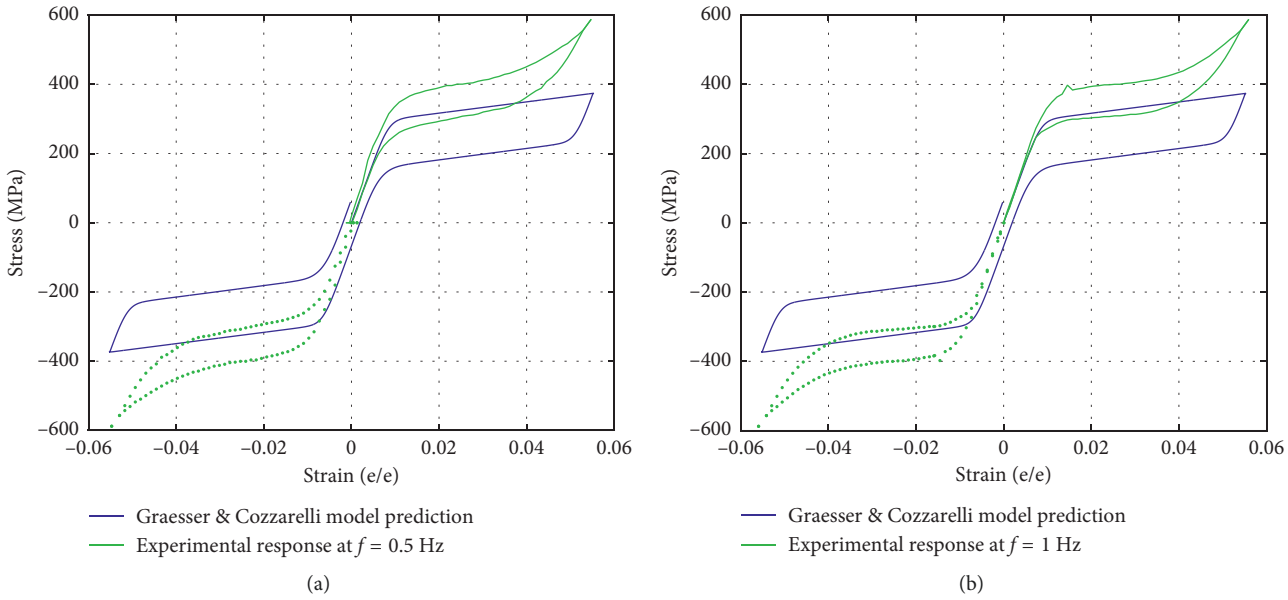

Figure 6: Comparison of Graesser – Cozzarelli model prediction to experimental response at (a) $f = 0.5$ Hz and (b) $f = 1$ Hz.

Here, $\Delta\sigma_2$ is the stress difference at the maximum strain between the experimental response at a frequency of 0.5 Hz and at a frequency of 0.025 Hz, $\dot{\varepsilon}_0$ is the strain rate produced by the frequency of 0.025 Hz, which corresponds to quasi-static conditions, and $\dot{\varepsilon}$ is the strain rate induced by the frequency in the dynamic range (0.5 Hz).

Comparison of the proposed model prediction to the experimental response at a frequency of 0.025 Hz, which corresponds to quasi-static conditions, shows that the elastic loading of martensite is well captured and that the overall behavior approximates the test data in an adequate manner. As far as the dynamic conditions are concerned, comparing the proposed model prediction to the experimental response at frequencies of 0.05 and 1 Hz, it is readily perceived that the influence of strain rate is also captured. These findings are presented in Figures 7 and 8, respectively, obtained by the procedure explained later.

In order to obtain the above results, a MATLAB code was utilised (not presented herein for brevity), while the experimental evidence was digitized from [11], and our findings were scale-fitted for an adequate comparison.

4. A Simple Application

Special truss moment frames (STMFs) are a rather new type of steel structural system that was developed for resisting forces and deformations induced by severe earthquake ground motions [12]. This system dissipates energy through ductile special segments located near the midspan of the truss girders. Essentially, the columns and truss segments are designed to remain elastic under forces that are generated by the fully yielded and strain-hardened special segments. For specific performance-based design criteria, one may refer to the UMCEE report by Chao and Goel [4], which recently have, with slight changes and additions, been incorporated in the ANSI/AISC 2016 Seismic Provisions [13].

Another type of truss moment frame, namely, the DTMF (Ductile TMF), was proposed by Longo et al. [14, 15]. This type provides energy dissipation via special devices located at the ends of the truss girders at the bottom chord level. Based on the kinematic theorem of plastic collapse, the best seismic performance is reached when, at the instance of collapse, all the dissipative devices have yielded while all the other members are in the elastic range (development of a global mechanism). However, the special devices used follow a rigid-plastic behavior, and hence, SMAs are excluded.

Traditional or dual-moment resisting frames are also a successful alternative in steel buildings [16–18], but there is "no room" of using dissipation devices in these since they provide seismic energy absorption mechanisms inherently.

Herein, we consider an STMF with a Vierendeel middle segment [3], improved by the placement of an SMA bar as a dissipation device diagonally in the special segment, namely, connecting joints J and D in the configuration shown in Figure 9. A time-dependent lateral load acts upon the frame along the top chord.

The columns and the members outside the special segment are designed to respond elastically, and plastic hinges will form only in the chord members and more specifically at the end of the middle segment, i.e., at points J, C, D, and L.

In what follows, the STMF is simulated via a 2-DOF mechanical model, based on certain simplifying assumptions. First, the mass of the beams is considered to be concentrated at the top of the column (lumped-mass model) neglecting the mass of the column. Second, a linear elastic response for all the members of the frame is considered. Column masses have finite rotational inertia, while all the masses of the other members of the frame have infinite rotational inertia. The axial deformation of the columns is insignificant, thus neglected. The columns and the beams

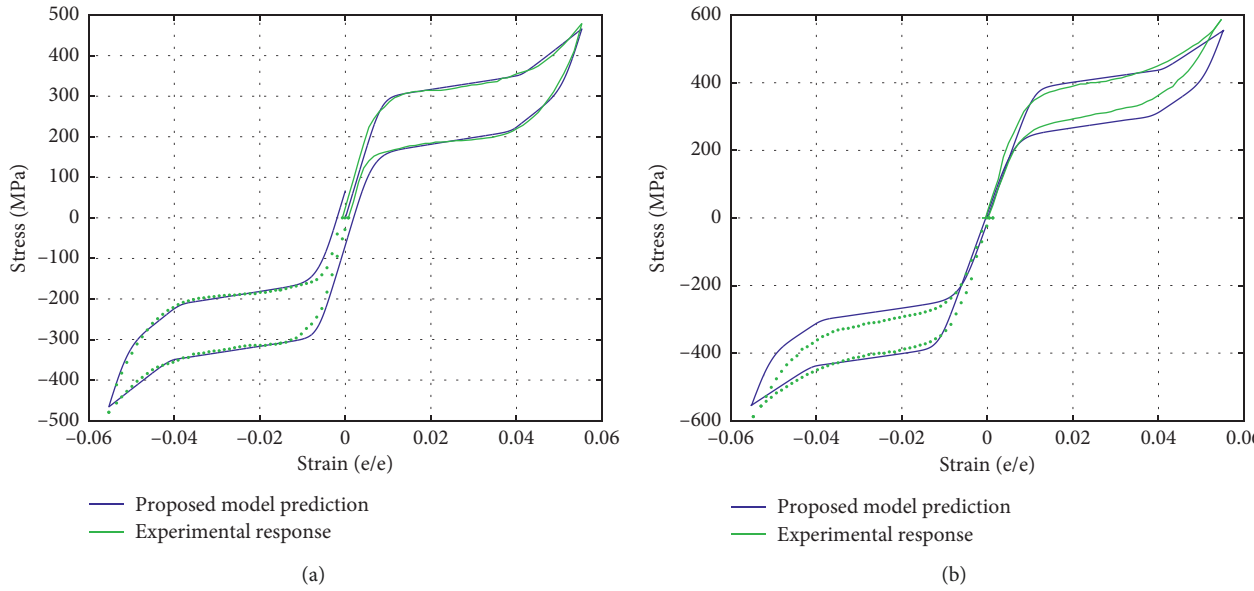

Figure 7: Comparison of the proposed model prediction to experimental response at frequencies (a) of 0.025 Hz and (b) of 0.5 Hz.

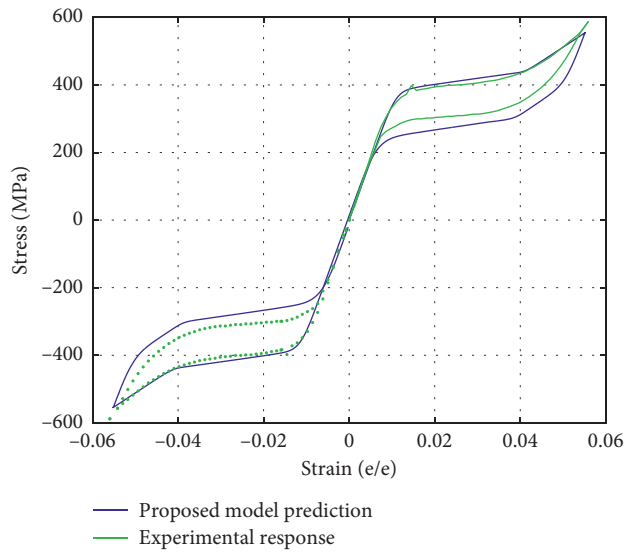

Figure 8: Comparison of the proposed model prediction to experimental response at a frequency of 1 Hz.

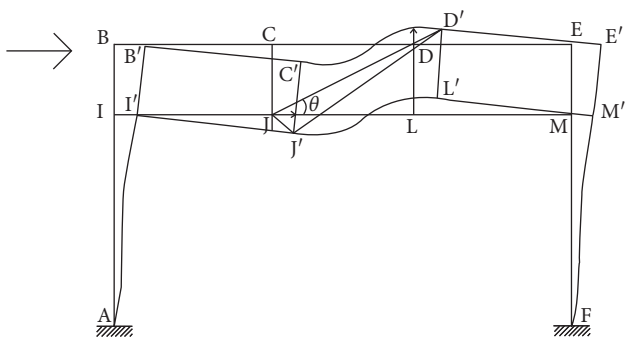

Figure 9: The undeformed and the deformed shape of the STMF configuration.

attached to them preserve their verticality and their initial length. The energy-dissipating device undergoes axial deformations. The lumped mass can move horizontally and can also rotate; hence, the generalized coordinates (degrees of freedom) are the horizontal translation and the rotation. In Figure 10, the lumped-mass model and the corresponding free body diagram are shown, accounting for the above assumptions.

The generalized forces exerted on the model are: the inertial moment M_{I}, the elastic moment of the column $M_{c,\varphi}$ (due to the rotation $\varphi(t)$), the elastic moment of the column $M_{c,ux}$ (due to the horizontal translation u_x), the spring force of the column $F_{C,ux}$ (due to u_x), and the vertical and horizontal components of the damping forces $F_{\mathrm{D}}^{\mathrm{V}}$ and $F_{\mathrm{D}}^{\mathrm{H}}$. These damping forces are calculated by integrating Equation (1), using the back stress expression of Equations (6)–(8) and converting in force units. The equations of motion are formulated and integrated in order to calculate forces and displacements. These equations can be found in a recent publication [19]. The members of the frame outside the special segment remain in the elastic range, and this is achieved by considering an elastic stiffness matrix.

Thereafter, the dynamic response of the model is studied under various types of simple time-dependent loading, as reported below.

4.1. Step Loading of Infinite Duration. Under the action of a lateral step load of infinite duration (of 10 kN), the damper dissipates some of the input energy and, finally, the system equilibrates in a deformed (point attractor) configuration as shown throughout Figures 11 and 12.

4.2. Decreasing Load Followed by Free Vibration. A load with decreasing amplitude of finite duration, starting from 9 kN and decaying linearly (followed by the model's free

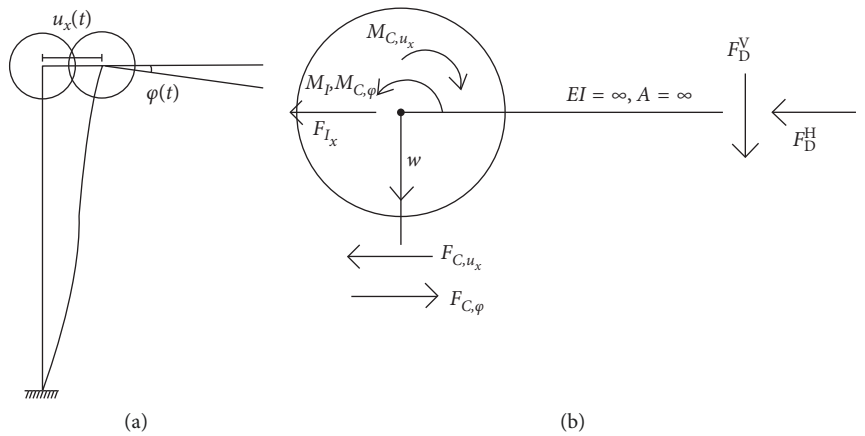

Figure 10: The 2-DOF lumped-mass mechanical model (a) and its free body diagram (b).

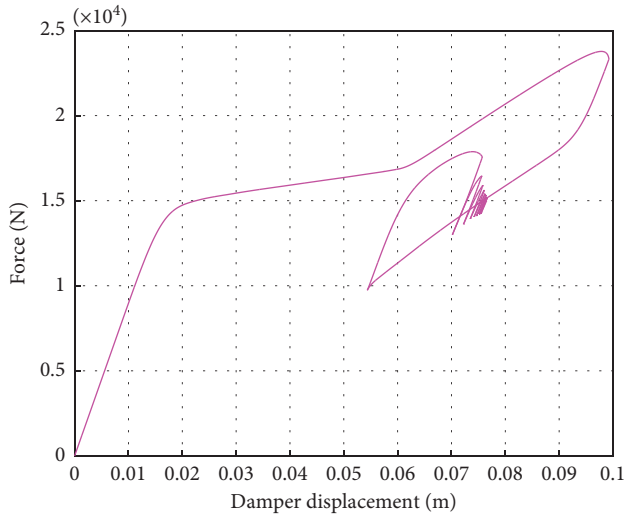

Figure 11: Damper response.

vibration) is studied here. Figure 13 illustrates the time history of the applied load and the damper response. The model returns to a position of a 1.8 mm horizontal displacement and zero rotation, as depicted in Figure 14.

4.3. Random Loading. A load derived by superposing random sinusoidal loads is applied to the model for 10 seconds. Afterwards, the model vibrates freely for 15 seconds, according to the contents of Figure 15. As depicted in Figure 16, the model returns to its undeformed shape, exhibiting a point attractor at the origin.

From the above results, a rather expected and well-captured response is reported. Future work (ongoing by the authors) involves (a) full-scale tests, (b) more sophisticated models, and (c) analyses via FE software, in order to fully validate the proposed model.

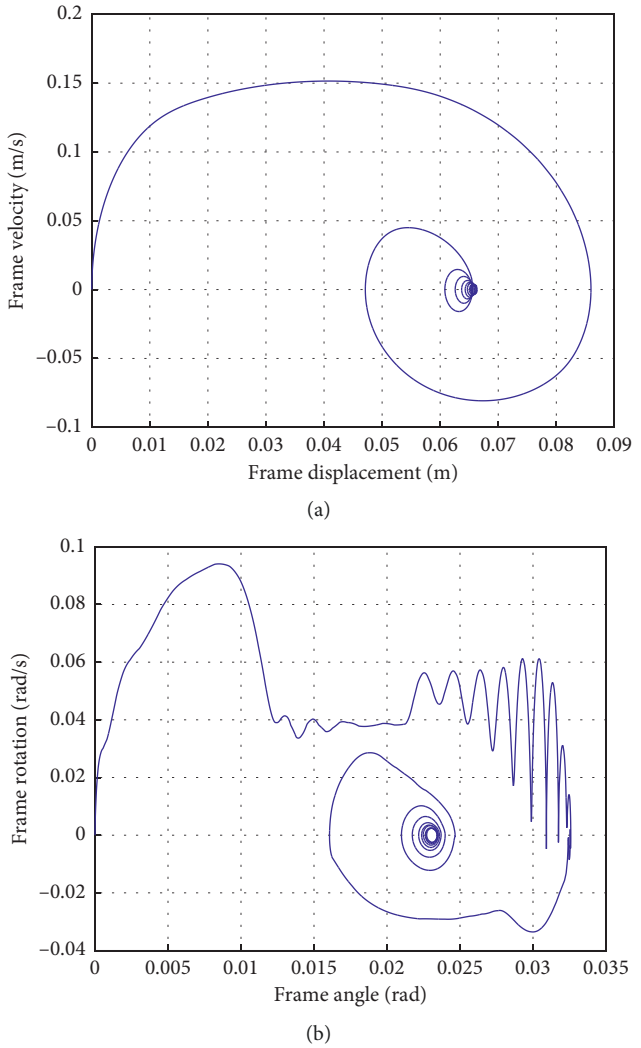

Figure 12: Displacement-velocity phase plane (a) and angle-rotation phase plane (b).

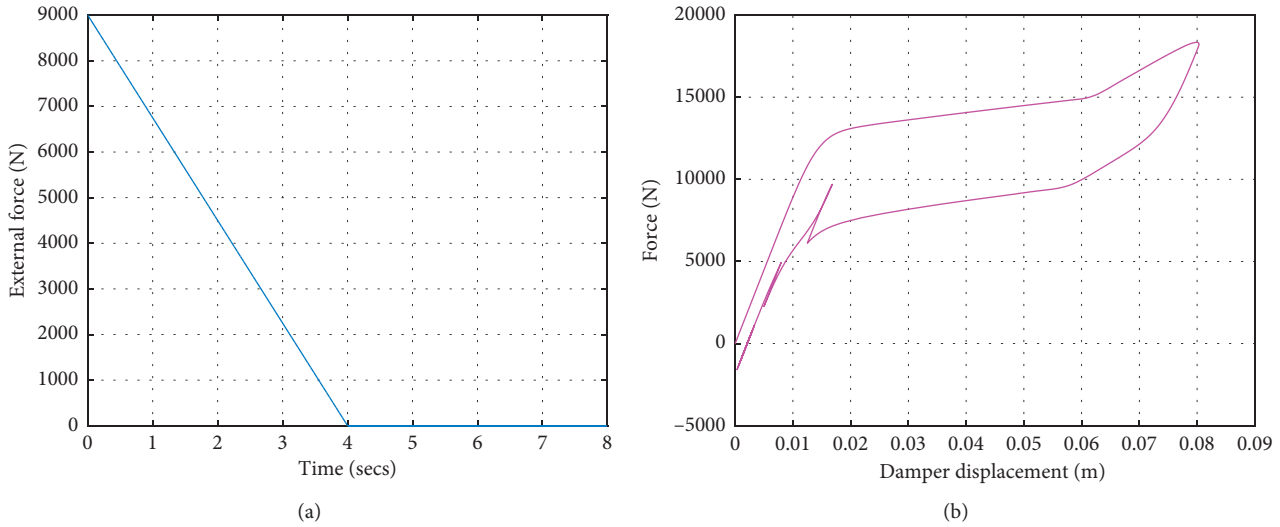

Figure 13: Decreasing load followed by free vibration. External load (a) and damper response (b).

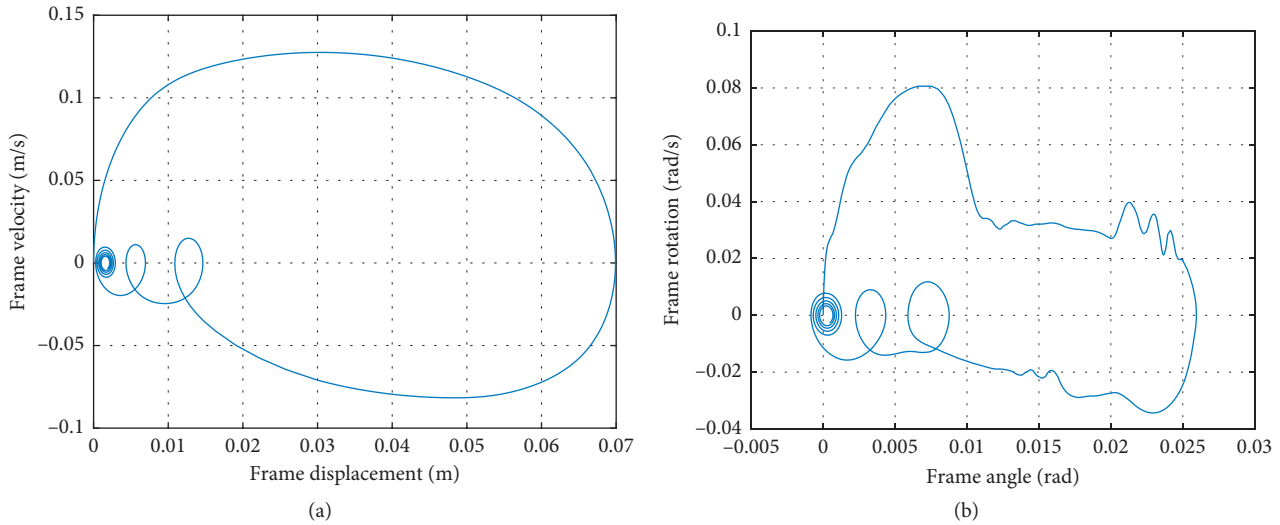

Figure 14: Decreasing load followed by free vibration. (a) The displacement-velocity phase plane and (b) the angle-rotation phase plane.

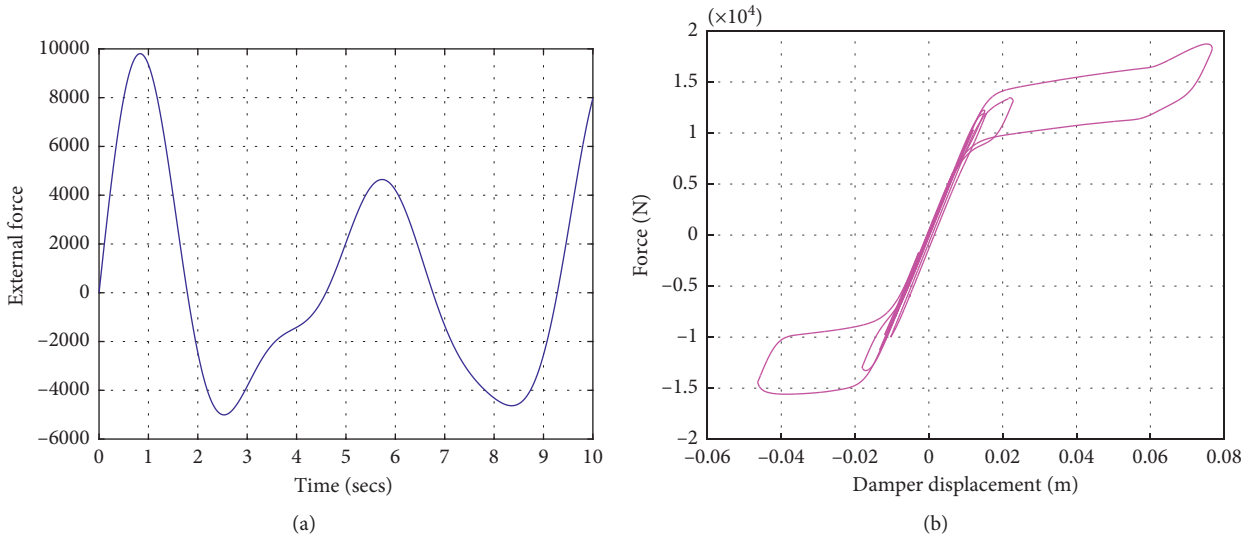

Figure 15: Random load followed by free vibration. (a) The external force applied and (b) the damper response.

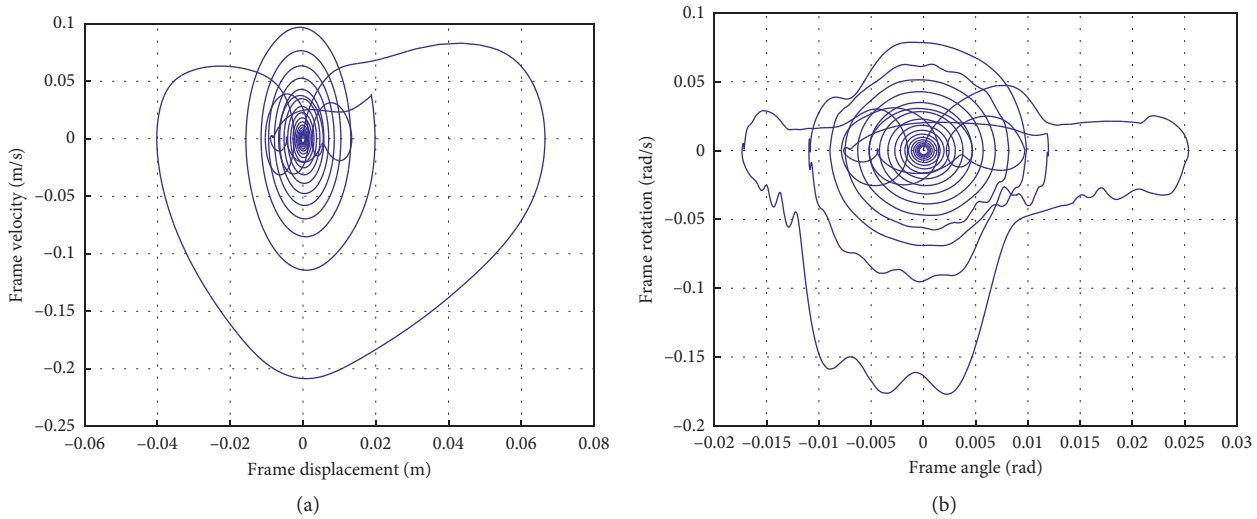

(a) (b)

Figure 16: Random load followed by free vibration. (a) The displacement-velocity phase plane and (b) the angle-rotation phase plane.

5. Conclusions

In this paper, after developing a new rate-dependent constitutive model of superelastic SMA bars, found in a very good agreement with existing experimental results, a 2-degree-of-freedom simulation is proposed, in order to capture the dynamics of a special truss moment frame simulation with an SMA bar incorporated, in an adequate manner. The model, giving satisfactory results for the loads under which it is acted upon, may be used to further examine the behavior of the STMF under loads that are more complicated and on multistory buildings, constituting the basis for ongoing research.

Data Availability

The data used to support the findings of this study are available from the corresponding author upon request.

Conflicts of Interest

The authors declare that they have no conflicts of interest.

References

[1] G. Song, M. Ma, and H.-N. Li, "Applications of shape memory alloys in civil structures," *Engineering Structures*, vol. 28, no. 9, pp. 1266–1274, 2006.

[2] R. Paiva and M. A. Savi, "An overview of constitutive models for shape memory alloys," *Mathematical Problems in Engineering*, vol. 2006, Article ID 56876, 30 pages, 2006.

[3] H. S. Basha and S. C. Goel, "Special truss moment frames with Vierendeel middle panel," *Engineering Structures*, vol. 17, no. 5, pp. 352–358, 1995.

[4] S. H. Chao and S. C. Goel, "Performance-based plastic design of seismic resistance special truss moment frames," Research Report UMCEE 06-03, Department of Civil and Environmental Engineering, The University of Michigan, Ann Arbor, MI, USA, May 2006.

[5] E. J. Graesser and F. A. Cozzarelli, "Multidimensional models of hysteretic material behavior for vibration analysis of shape memory alloys," Technical Report NCEER-89-0018, State University of New York at Buffalo, Buffalo, NY, USA, 1989.

[6] D. C. Lagoudas, *Shape Memory Alloys. Modeling and Engineering Applications*, Springer, New York, NY, USA, 2008.

[7] W. J. Buehler, J. V. Gilfrich, and R. C. Wiley, "Effect of low-temperature phase changes on the mechanical properties of alloys near composition of NiTi," *Journal of Applied Physics*, vol. 34, no. 5, pp. 1475–1477, 1963.

[8] H. Özdemir, "Nonlinear transient dynamic analysis of yielding structures," Ph.D. dissertation, University of California, Berkeley, CA, USA, 1976.

[9] K. Wilde, P. Gardoni, and Y Fujino, "Base isolation system with shape memory alloy device for elevated highway bridges," *Engineering Structures*, vol. 22, no. 3, pp. 222–229, 2000.

[10] F. Auricchio, D. Fugazza, and R. DesRoches, "A 1D rate-dependent viscous constitutive model for shape-memory alloys: formulation and comparison with experimental data," *Smart Materials and Structures*, vol. 16, no. 1, pp. 39–50, 2007.

[11] R. DesRoches, J. McCormick, and M. Delemont, "Cyclic response of superelastic shape memory alloy wires and bars," *Journal of Structural Engineering*, vol. 130, no. 1, pp. 38–46, 2004.

[12] S. C. Goel and A. M. Itani, "Seismic-resistant special truss-moment frames," *Journal of Structural Engineering*, vol. 120, no. 6, pp. 1781–1797, 1994.

[13] ANSI, *ANSI/AISC 341-16: Seismic Provisions for Structural Steel Buildings*, American Institute of Steel Construction, Chicago, IL, USA, 2016.

[14] A. Longo, R. Montuori, and V. Piluso, "Theory of plastic mechanism control of dissipative truss moment frames," *Engineering Structures*, vol. 37, pp. 63–75, 2012.

[15] A. Longo, R. Montuori, and V. Piluso, "Failure mode control and seismic response of dissipative truss moment frames," *Journal of Structural Engineering*, vol. 138, no. 11, pp. 1388–1397, 2012.

[16] R. Montuori, E. Nastri, and V. Piluso, "Advances in theory of plastic mechanism control: closed- form solution for MR-frames," *Earthquake Engineering & Structural Dynamics*, vol. 44, no. 7, pp. 1035–1044, 2015.

[17] D. Cassiano, M. D'Aniello, C. Rebelo, R. Landolfo, and L. Simoes da Silva, "Influence of seismic design rules on the

robustness of steel moment resisting frames," *Steel and Composite Structures*, vol. 21, no. 3, pp. 479–500, 2016.

[18] A. Techini, M. D'Aniello, C. Rebelo, R. Landolfo, L. Simoes da Silva, and L. Lima, "Seismic performance of dual-steel moment resisting frames," *Journal of Constructional Steel Research*, vol. 101, pp. 437–454, 2014.

[19] M. Ntina, D. Sophianopoulos, and P. Tsopelas, "Development of a 2-dof model simulating the dynamic response of special truss moment frames with shape memory alloy bars as dissipation devices in the special segment," in *Proceedings of Eurosteel 2017*, Copenhagen, Denmark, September 2017.